Chinese Chemical Letters 33 (2022) 1025–1031

Contents lists available at ScienceDirect

Chinese Chemical Letters

journal homepage: www.elsevier.com/locate/cclet

A hybrid lithium sulfonated polyoxadiazole derived single-ion conducting gel polymer electrolyte enabled effective suppression of dendritic lithium growth

Dazhe Li[a], Longbo Luo[a], Jiadeng Zhu[b], Haimei Qin[c], Pengqing Liu[a], Zhaomei Sun[a], Yi Lei[a], Mengjin Jiang[a,*]

[a] College of Polymer Science & Engineering, Sichuan University, Chengdu 610065, China
[b] Chemical Sciences Division, Oak Ridge National Laboratory, Oak Ridge, TN 37831, United States
[c] State Key Laboratory for Physical Chemistry of Solid Surfaces, Fujian Provincial Key Lab of Theoretical and Computational Chemistry, and College of Chemistry and Chemical Engineering, Xiamen University, Xiamen 361005, China

ARTICLE INFO

Article history:
Received 5 June 2021
Revised 4 July 2021
Accepted 6 July 2021
Available online 13 July 2021

Keywords:
Polyoxadiazole sulfonate
Single-ion conductor
Gel polymer electrolyte
Lithium dendrite
Lithium metal battery

ABSTRACT

Lithium metal is deemed as an ideal anode material in lithium-ion batteries because of its ultrahigh theoretical specific capacity and the lowest redox potential. However, the rapid capacity attenuation and inferior security resulting from the dendritic lithium growth severely limit its commercialization. Herein a novel hybrid gel polymer electrolyte (GPE) based on electrospun lithium sulfonated polyoxadiazole (Li-SPOD) nanofibrous membrane swelled by lithium bis(trifluoromethanesulfonyl)imide (LiTFSI) ether liquid electrolyte is proposed to address the issue of lithium dendrites. The Li-SPOD membrane synthesized by a simple one-pot method exhibits excellent mechanical strength and thermal resistance due to its high molecular weight and rigid backbone. The electron-withdrawing oxadiazole ring and oxadiazole ring-Li^+ complex, and N, O heteroatoms with lone pairs of electrons in Li-SPOD macromolecular chains facilitate the dissociation of -SO_3Li group and Li^+ transference. The hybrid Li-SPOD GPE exhibits both a high lithium-ion transference number (0.64) and high ionic conductivity (2.03 mS/cm) as well as superior interfacial compacity with lithium anodes. The $LiFePO_4$-Li cell using this novel GPE can operate steadily at 2 C for 300 cycles, remaining a high discharge capacity of 125 mAh/g and dendrite-free anode. Remarkable performance improvements for the Li-Li and Cu-Li cells are also presented.

The rapid developments of portable electronics and electric vehicle industry have driven rechargeable lithium metal batteries (LMBs) that use lithium metal as the anode to be one of the most concerned research hotspots of energy storage in recent years due to its extremely high theoretical specific capacity (3860 mAh/g) and lowest redox potential (−3.04 V *vs.* standard hydrogen electrode) [1,2]. However, during the repeated charging/discharging process, uncontrollable lithium dendrite proliferation resulting from the inhomogeneous Li^+ deposition on the surface of lithium anode not only leads to low coulombic efficiency (CE) and consumption of electrolyte induced by the high reactivity of lithium metal, but also results in potential security issues [3,4].

Various strategies have been proposed to suppress the growth of lithium dendrites, including three-dimensional porous collectors, artificial solid electrolyte interphase (SEI) layers, separators with high moduli and homogeneous pore structures, and single lithium-ion conducting gel polymer electrolytes (GPEs), *etc.* [4–7]. Polyanion-based GPEs possess high lithium-ion transference numbers (t_{Li^+}) that approach unity by immobilizing anions on the polymer skeleton, which can effectively prevent anion depletion near the lithium electrode and formation of lithium dendrites [8,9]. Compared with the polyanions based on carboxylates, sulfonylimides, and tetrahedral borates, polymeric sulfonates are featured as high anodic stability, moderate negative charge distribution and facile synthesis [8–10]. Among various sulfonate-based polyanions, the most widely used polymeric sulfonates in LMBs are lithiated fluoroalkyl-containing polymeric sulfonates, especially Nafion (Li-Nafion) [9,11,12], polystyrene sulfonate (Li-PSS) [13–15], and poly(2-acrylamide-2-methylpropane sulfonate) (Li-PAMPS) [16–18]. Despite the high ionic conductivity (σ) due to the strong electron-withdrawing effect of fluorine atoms, Li-Nafion is too expensive to be commercialized. Freestanding membranes are intractable to be

* Corresponding author.
E-mail address: memoggy@126.com (M. Jiang).

https://doi.org/10.1016/j.cclet.2021.07.021
1001-8417/

prepared from Li-PSS and Li-PAMPS owing to their low molecular weights and soft backbones [19].

According to the widely accepted space-charge theory, besides the high t_{Li^+}, a high σ is also essential for suppressing lithium dendrites [1,20]. Furthermore, the continuum theory claims that the driving force for the formation of lithium dendrites can be reduced by a factor of ten or more if as little as 10% of anions are fixed [7,21]. Thus, it is possible to employ polyanions with relatively low negative charge delocalization for effective dendrite inhibition through swelling the single lithium-ion conducting polyanions with liquid electrolytes to prepare ionomer-liquid electrolyte hybrid GPEs [22–24], in which much higher σs can be obtained at a small expense of t_{Li^+}s. For example, the t_{Li^+} (0.72) and σ (0.45 mS/cm) of the polyethylene-supported Li-PSS/$LiPF_6$ ester liquid electrolyte hybrid GPE are 1.67 times and 1.5 times higher than those of the $LiPF_6$ ester liquid electrolyte, respectively, so that the lithium dendrites are dramatically suppressed [14]. The high t_{Li^+}s of the hybrid GPEs are mainly ascribed to the strong electrostatic repulsion of the immovable polyanions towards the small anions in the liquid electrolytes [14]. This principle is also exploited to suppress polysulfides' shuttle in lithium-sulfur batteries [18,24,25].

Sulfonated aromatic polyoxadiazoles (SPODs) are one kind of extensively studied proton conducting materials for fuel cells [26,27]. In comparison with the sulfonated polymers mentioned above, the SPODs possess the four unique merits [26–30]: (1) high sulfonation degree and molecular weight are simultaneously obtained through a simple one-pot synthesis method in oleum; (2) a freestanding membrane with outstanding mechanical and thermal stability can be easily fabricated due to the high molecular weight and rigid backbone; (3) the electron deficiency of oxadiazole rings is expected to promote the delocalization of negative charge on the sulfonate groups; (4) the alkalescent nitrogen and oxygen atoms with lone pairs of electrons provide a large number of electrostatic attraction points for the desolvation and hopping of cations. All of these enable SPODs strong competitors for the preparation of ionomer-liquid electrolyte hybrid GPEs.

In this work, a freestanding hybrid GPE membrane was fabricated by swelling the electrospun lithium sulfonated polyoxadiazole (Li-SPOD) nanofiber membrane with lithium bis(trifluoromethanesulfonyl)imide (LiTFSI) ether liquid electrolyte. The Li-SPOD/LiTFSI hybrid GPE with high anodic stability possesses an excellent dendrite-inhibiting effect on the lithium metal anode due to its high t_{Li^+} and σ. As a result, remarkable cycling performance improvements are achieved for $LiFePO_4$-Li, Li-Li and Cu-Li cells with such unique GPEs. Its superb dendrite-suppressing ability, simple synthesis method and outstanding mechanical strength demonstrate that this novel hybrid GPE has broad application prospects in rechargeable LMBs.

The ATR-FTIR spectrum of the electrospun Li-SPOD membrane is shown in Fig. 1a, where the two peaks at 1088 and 1605 cm^{-1} correspond to the =C–O–C= and C=N stretching vibration of oxadiazole rings [27,31]. The SO and SO_2 stretches of sulfonate groups give rise to the peaks at 736, 1031 and 1396 cm^{-1} [27,32]. The broad characteristic bands between 1130 and 1345 cm^{-1} are ascribed to the C–O–C stretch of diphenyl ether groups and the SO_2 stretch of the phenoxathiine rings and the lithium sulfonate groups [27,31,33]. The peak at 1464 cm^{-1} is assigned to the aromatic C=C stretch [27]. The complete cyclization of hydrazides to form the oxadiazole rings is confirmed by the absence of signal peaks between 9.5 ppm and 11 ppm in the ^1H NMR spectrum [27,34] (Fig. 1b), despite the failure to determine the composition of the copolymer owing to the overlapping of some aromatic hydrogen peaks [27,33]. Due to the oleum's powerful sulfonation ability, all the phenylenes are sulfonated during the polymerization process with some phenoxathiine rings formed *via* a further dehydration reaction between the sulfonate group and the α-hydrogen of adjacent phenylene, which is verified by the result of EA. As shown in Table S1 (Supporting information), the measured atomic ratios of N/C and S/C are almost the same as those obtained from the proposed chemical structure in Fig. 1b. Such high sulfonation degree is challenging to be achieved by traditional post-sulfonation methods. Besides, the number-average molecular weight ($\bar{M}_n$) and weight-average molecular weight ($\bar{M}_w$) of Li-SPOD determined by GPC are up to 1.62×10^5 and 3.41×10^5, respectively, which are much higher than those of Li-PSS [18] and lithium sulfonated polyether ether ketone (Li-SPEEK) [35].

As summarized in Table S2 (Supporting information), the porosity (81.2%) of the electrospun Li-SPOD nanofibrous membrane measured by the *n*-butanol uptake method is much higher than that (40.7%) of the PP separator, which is beneficial to the liquid electrolyte uptake. The macromolecular aggregation state of the electrospun nanofibrous Li-SPOD membrane swelled by the LiTFSI ether liquid electrolyte [36,37] was analyzed through XRD. As shown in Fig. 1c, while all the three membranes exhibit amorphous XRD peaks, the peak of Li-SPOD GPE is flatter, implying higher randomness of molecular stacking due to the permeation of solvents and ions. The amorphous structure would facilitate the diffusion of solvents and ions into the nanofibers [38,39]. The microtopography of Li-SPOD nanofibers swelled by liquid electrolyte can be directly observed by SEM images (Fig. 1e). The average diameter (D) of the swelled nanofibers is 33.9% larger than that of the as-prepared electrospun Li-SPOD nanofibers (Fig. 1d). Unlike the loose three-dimensional network in the as-prepared electrospun membrane with many large pores, nanofibers in the liquid electrolyte treated membrane arrange very densely, and many adhesion points between the nanofibers can be found.

Owing to its high molecular weight and rigid backbone, the Li-SPOD possesses outstanding mechanical strength. As shown in Fig. 1f, the tensile strength of the as-prepared electrospun Li-SPOD membrane (10.2 MPa) is nearly the same as that of the Celgard-2500 in the transverse direction (TD) (Fig. S2 in Supporting information), while that of the Li-SPOD nanofiber hybrid GPE further increases to 14.2 MPa due to the adhesion of swelled nanofibers with each other. Moreover, the tensile strength of the dense Li-SPOD membrane (41.9 MPa) displays a tremendous advantage over those of Li-PAMPS based on a PVDF backbone (~26 MPa) [40], Li-Nafion (~10 MPa) and Li-SPEEK (~13.2 MPa) [41]. In addition, the electrospun Li-SPOD nanofiber membrane exhibits excellent heat resistance with an initial thermal degradation temperature of ~472 °C in nitrogen (Fig. S3 in Supporting information). It is able to maintain its dimensional stability even at a temperature of higher than 350 °C in the air (Fig. S4 in Supporting information), which can prevent the cell from the internal short at an elevated operation temperature [42,43].

The abundant -SO_3Li groups and N, O heteroatoms, and amorphous structure are expected to endow the Li-SPOD membranes with superb wettability to the liquid electrolyte, which is demonstrated by the result of contact angle measurement, as shown in Fig. 2a and Table S2 (Supporting information). The electrolyte drop was wholly absorbed by the Li-SPOD nanofiber membrane instantly so that the contact angle of 0° was recorded. The Li-SPOD dense membrane's contact angle toward the liquid electrolyte is 24.6°, which is much lower than that of Celgard-2500 membrane (34.3°). Besides, the liquid electrolyte uptake of Li-SPOD nanofiber membrane (586.1%) is much higher than that of Celgard-2500 (129.3%) because of the excellent wettability and the high porosity of the electrospun membrane.

It is reported that the electron-deficient oxadiazole heterocycle possesses an electron-withdrawing ability comparable to those of sulfone and ketone groups [29,30], which is expected to prompt negative charge distribution on the sulfonate anion, and therefore facilitate the dissociation of -SO_3Li group. DFT calculations proved

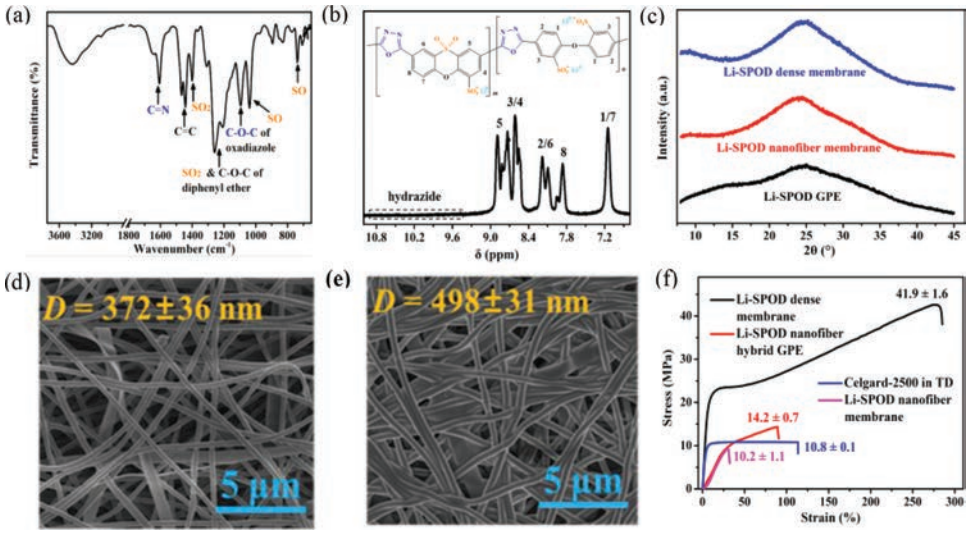

Fig. 1. (a) The ATR-FTIR and (b) ^{1}H NMR spectrums of Li-SPOD. (c) XRD patterns of different Li-SPOD membranes. SEM images of Li-SPOD nanofiber membranes (d) before and (e) after swelling in the liquid electrolyte. (f) Typical stress-strain curves of different membranes.

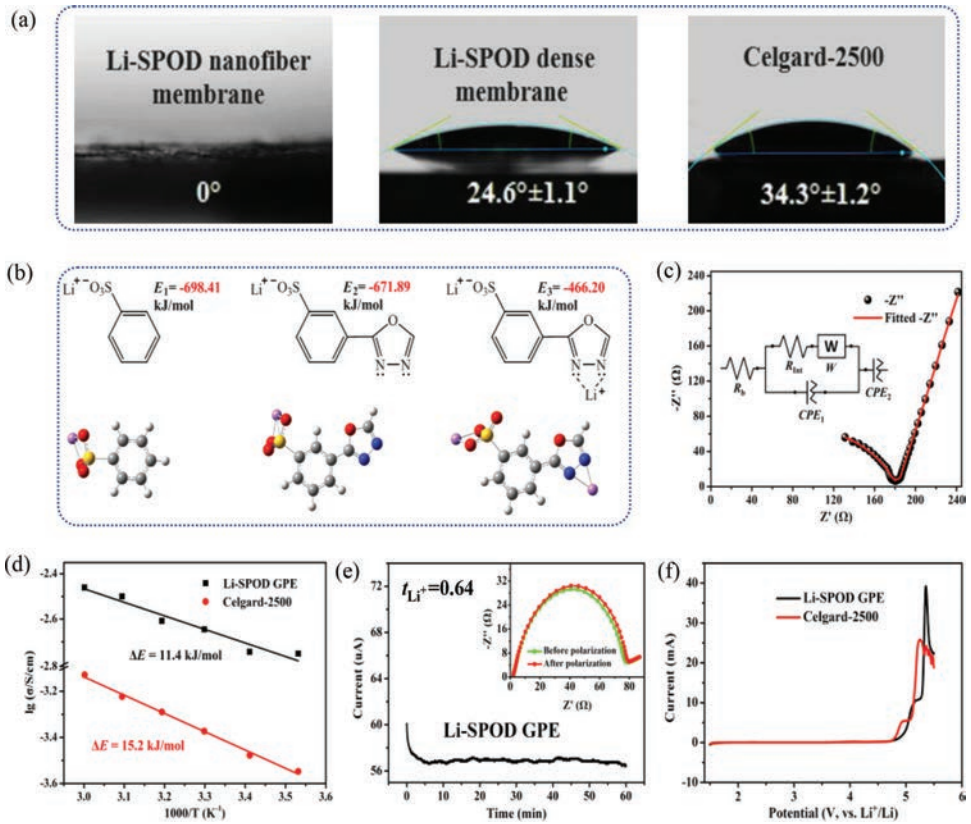

Fig. 2. (a) Liquid electrolyte contact angles of different membranes, (b) results of DFT calculations, (c) Nyquist plot of the Li-SPOD nanofiber membrane swelled by the mixed ether solvent sandwiched between two SS blocking electrodes and the corresponding equivalent circuit (the inset), (d) ionic conductivities at different temperatures (correlation between the conductivity and the temperature), (e) current-time curve for the Li-Li symmetric cell with the Li-SPOD GPE and the Nyquist plot (the inset) before and after polarization, and (f) LSV curves for the measurement of ESWs.

this feature. As shown in Fig. 2b, althrough the lithium ionic binding energy of the sulfonate in the model structure with an oxadiazole meta-substituent (E_2 = 671.891 kJ/mol) is only slightly lower than that of benzenesulfonate (E_1 = 698.41 kJ/mol), the lithium ionic binding energy of the sulfonate sharply decreases to E_3 = 466.20 kJ/mol, which is 33.2% lower than E_1, when the alkalescence oxadiazole ring adsorbs one Li^+, indicating a unique advantage of Li-SPOD over other lithium polysulfonates, such as Li-PSS and Li-PAMPS. Moreover, the interesting find that the oxadiazole ring-Li^+ complex can significantly promote the ionic dissociation of the -SO_3Li group may arouse a new insight on the proton-conducting mechanism of sulfonated aromatic heterocyclic polymers considering the similarity between the Li^+ ions and protons [44].

To further illustrate the ionic dissociation of Li-SPOD, the ionic conductivity of the Li-SPOD nanofiber membrane swelled by the

mixed ether solvent for 72 h was measured through an SS-SS blocking cell. As shown in Fig. 2c, the Nyquist plot comprises an arc in the high-frequency region caused by the interfacial resistance (R_{int}), and an inclined straight line at the lower frequency associated with the Warburg resistance (W). The plot is well fitted with an equivalent circuit (the inset), in which R_b represents the bulk resistance of the pure Li-SPOD single-ion conducting GPE (SIC-GPE). The R_b, R_{Int} and corresponding ionic conductivities are summarized in Table S3 (Supporting information). The bulk conductivity (σ_b) and conductivity calculated based on R_b + R_{Int} ($\sigma_{(b+Int)}$) are 0.352 and 0.0208 mS/cm at 25 °C, respectively. The σ_b of Li-SPOD-based SIC-GPE is much higher than those of the reported Li-PSS [19] and AMPSLi-g-PVDF-HFP [17] based nanofibrous SIC-GPEs, which are only 0.02–0.06 and 0.034 mS/cm at 30 °C, respectively. It is even comparable to that of the lithium poly[4-styrenesulfonyl(phenylsulfonyl)imide]/PVDF based dense SIC-GPE (0.57 mS/cm at room temperature) [45]. The high σ_b of Li-SPOD-based SIC-GPE means a high degree of ionic dissociation, which can be ascribed to the electron-withdrawing effect of the oxadiazole ring and the oxadiazole ring-Li^+ complex, and the high specific surface area of the nanofibers.

The σ and t_{Li^+} are two essential parameters to assess the ionic transport property of electrolytes. As shown in Table S2, the σ of hybrid Li-SPOD GPE is 2.03 mS/cm, which is more than 5 times that of the liquid electrolyte filled in the PP separator (0.38 mS/cm). Correspondingly, the ionic migration activation energy (ΔE) for the hybrid GPE (11.4 kJ/mol) calculated according to the Arrhenius formula is 25% lower than that for the PP separator (15.2 kJ/mol), implying the more facilitated ionic movement in the former [46], as depicted in Fig. 2d. The conductivity enhancement mainly arises from the better wetting affinity and the higher electrolyte uptake of hybrid GPE.

Similar to the values in the literature [18,47], the t_{Li^+} of LiTFSI liquid electrolyte in the PP membrane measured is 0.41, while that of the hybrid Li-SPOD GPE is 0.64 (Table S2, Fig. 2e and Fig. S5 in Supporting information). The dissociation of -SO_3Li in the Li-SPOD-based hybrid GPE mentioned above can retard the $TFSI^-$ movement by electrostatic repulsion from the anchored polyanions, and provide more free Li ions. Besides, the electrostatic attraction between Li ions and the unshared electron pairs on nitrogen and oxygen atoms is conducive to the desolvation of strongly solvated Li ions [24], as shown in Fig. 3e (left). All these factors make contributions to the superior lithium-ion transferability of the hybrid GPE. The electrochemical stability window (ESW), as an essential aspect of GPEs, was investigated by LSV. According to Fig. 2f, the ESW of the hybrid Li-SPOD GPE (4.75 V) is slightly higher than that of the pure LiTFSI liquid electrolyte filled in the PP microporous membrane (4.70 V), indicating a retardation effect of Li-SPOD on liquid electrolyte decomposition [48].

The interfacial compatibility of the GPE with lithium anodes is a significant parameter determining the cycle life of lithium metal anode-based batteries, which was evaluated by the static impedance change of Li-Li symmetric cells with time at 25 °C. An equivalent circuit (Fig. S6c in Supporting information) [49] is used to fit the Nyquist plot (Fig. S6a in Supporting information), in which the semicircle and the intercept at high frequency represent the interfacial resistance (R_{Int}) and bulk resistance (R_b), respectively. As shown in Fig. S6b (Supporting information), the cell with the hybrid Li-SPOD GPE exhibits lower interfacial resistances all through the 7 days compared to the cell using Celgard-2500, demonstrating its better interfacial compatibility. The initial increase of R_{Int} is ascribed to the formation and thickening of the SEI passivation layer, which is stabilized subsequently by the $LiNO_3$ additive [50,51]. Corresponding to the higher ionic conductivity of the hybrid GPE, the R_b of the GPE here is lower than that of the PP separator as well.

The $LiFePO_4$-Li cells with such a unique membrane were assembled and tested to investigate the application performance of prepared GPE. The cell with the hybrid Li-SPOD GPE possesses higher discharge capacities than that using Celgard-2500 (Fig. 3a), especially at 4 C, which is up to a significant increase of 23.1%. The corresponding charge/discharge profiles are shown in Fig. S7 (Supporting information). The voltage plateau difference, hysteresis voltage, reflects the total internal resistance (R_b + polarization resistance) of the cells, in which the polarization resistance plays a dominant role as the R_b is relatively small [14]. As can be seen from Fig. 3b, although the hysteresis voltages of both cells rise with the increase of the current density, the hysteresis voltage of the cell with hybrid Li-SPOD GPE is lower than that of the cell using the PP separator, indicating smaller polarization resistance for the former. Moreover, similar to the capacity difference, the difference of hysteresis voltage between the two cells is also roughly proportional to the current density, implying that the hybrid GPE exerts a more significant inhibiting effect on polarization at a higher current density. The higher t_{Li^+} can mitigate the anion accumulation in the vicinity of the cathode (Fig. 3e, middle), especially at high current densities, so that the resistance caused by the concentration polarization is low [14]. Besides, the much higher electrolyte uptake and ionic conductivity, and the better interface compatibility between lithium anodes and Li-SPOD GPE also contribute to the suppression of cell polarization. Hence the higher capacity retentions at higher current densities are obtained.

The $LiFePO_4$-Li half-cell with the hybrid Li-SPOD GPE also exhibits much better long-term cycling performance than that using Celgard-2500. As shown in Fig. 3d, the two cells display similar discharge capacities in the initial 60 cycles. The cell with the hybrid Li-SPOD GPE can keep stable capacities of higher than 125 mAh/g in the subsequent 240 cycles, while the capacities of the reference cell decline from 117.8 mAh/g at the 60th cycle to 101.1 mAh/g at the 300th cycle. Accordingly, the hysteresis voltage of the $LiFePO_4$-Li half-cell with the hybrid Li-SPOD GPE is much lower and increases much slower with the cycling time compared with that of the cell using Celgard-2500 (Fig. 3c and Fig. S8 in Supporting information).

The ionic concentration gradient between the two electrodes can not only result in the concentration polarization resistance, but also lead to the formation and proliferation of lithium dendrites, especially at higher current densities, because of local ionic depletion nearby the anode surface (Fig. 3e, middle), according to the space-charge model [1,7,52]. Therefore, a much more compact and smoother surface (Fig. 3e, right) of Li metal anode of the $LiFePO_4$-Li cell with the hybrid Li-SPOD GPE after 300 cycles at a current density of 2 C is found compared with that using the conventional PP separator, indicating a significant inhibiting effect of the high-t_{Li^+} GPE on lithium dendrites. The much slower increase of hysteresis voltage (Fig. 3c and Fig. S8) can also be deemed as a piece of circumstantial evidence for suppressing lithium dendrites, as the dendrite growth will boost internal resistance by consuming electrolyte and thickening the SEI passivation layer. Moreover, the plentiful alkalescent oxadiazole heterocycles may play a significant role in guiding the uniform lithium deposition [53,54], in addition to the better wettability and higher liquid electrolyte uptake.

The result [6,55–57] of XPS (Table S4 and Fig. S9 in Supporting information) shows no significant surface element difference between the two lithium metal anodes of the $LiFePO_4$-Li cells after 300 cycles at 2 C. This may be because a small amount of lithium dendrites also inevitably formed on the surface of the lithium metal anode with the Li-SPOD GPE separator, as implied by the gradually rising hysteresis voltage (Fig. 3c). Since our strategy is not to suppress lithium dendrites by design a novel SEI layer [1,55], the chemical structure of the outermost SEI layer keeps relatively

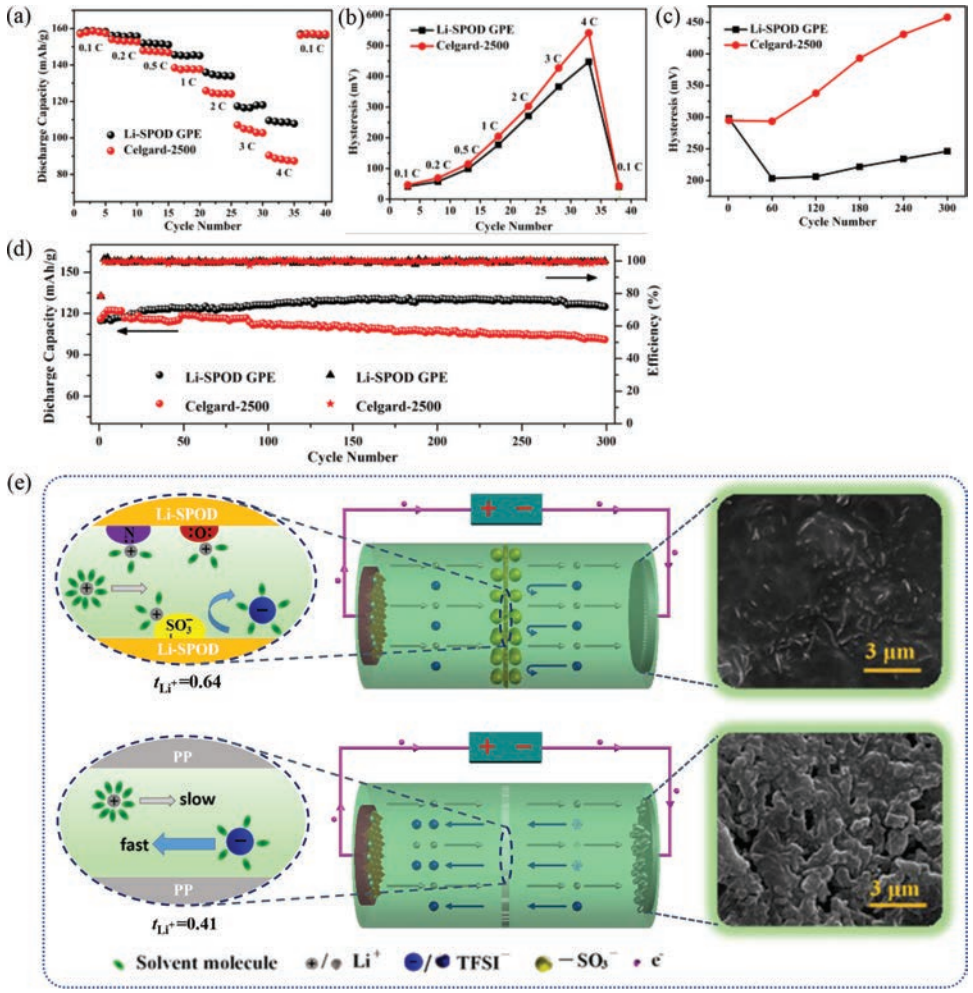

Fig. 3. (a) Rate capability and (b) hysteresis voltages at different current densities of the $LiFePO_4$-Li cells. (c) Hysteresis voltages and (d) cycling stability of the $LiFePO_4$-Li cells at a current density of 2 C. (e) Schematic profiles of ionic transport mechanism inside the $LiFePO_4$-Li cells during the charging process, and corresponding surface SEM images of Li anodes after 300 cycles at 2 C.

stable, regardless of the surface morphology of the lithium metal anodes.

The Li-SPOD GPE-based $LiFePO_4$-Li cell also possesses excellent cycling stability at an elevated temperature due to its outstanding heat resistance. As shown in Fig. S10 (Supporting information), after 90 cycles at 2 C under 60 °C, the capacity retention of the cell with Li-SPOD GPE is higher than 95%, while that of the Celgard-2500-based cell is only 83.4%. It is also found that the discharge capacities of both the two cells remarkably increase as the temperature rises from 25 °C to 60 °C, which is due to the reduced internal impedances in the electrolyte, cathode and interfaces between the electrolyte and electrodes at the higher temperature. In addition, the elevated temperature also leads to a slight reduction (~1%) of Coulombic efficiency, corresponding to more side reactions.

Cycling tests of Li-Li and Cu-Li cells were performed to validate the superiority of the hybrid Li-SPOD GPE in the performance improvement of lithium metal anode-based cells further. The Li-Li symmetric cell cycling test was conducted with a depositing/stripping capacity of 1 mAh/cm^2 at 2 mA/cm^2. As displayed in Fig. 4a, the two cells exhibit approximate hysteresis voltages in the initial 50 h. In the subsequent 350 h, the cell's hysteresis voltage with the Li-SPOD GPE gradually reduces to nearly a constant around 50 mV, while that of the cell using Celgard-2500 keeps increasing from ~100 mV to ~200 mV. The difference of hysteresis voltage between the two Li-Li cells is similar to that between the two $LiFePO_4$-Li cells, indicating the same outstanding dendrite inhibiting effect of the hybrid Li-SPOD GPE. The surface morphologies of Li electrodes of the Li-Li cells after 400 h cycling are shown in Fig. 4b. A much more compact and smoother surface of Li metal electrode with the hybrid Li-SPOD GPE is observed than that using the conventional PP separator. The more severe lithium dendrite proliferation during the cycling of Li-Li cells compared to that of the $LiFePO_4$-Li cells can be ascribed to the longer cycling time or increased cycling number and higher current density of the Li-Li cells.

The Coulombic efficiency (CE) of a Cu-Li cell directly reflects the dendrite growth as the fresh surface of newly generated dendritic lithium will react with electrolyte to form an SEI layer, resulting in an irreversible capacity loss. The fixed capacity deposited onto the Cu electrode in each cycle during the Cu-Li cells' cycling tests is 1 mAh/cm^2. As shown in Fig. 4c, at a low current density of 1 mA/cm^2, the cell with hybrid Li-SPOD GPE can maintain stable CEs of higher than 97% for 81 cycles, 44.6% longer than that for the cell using Celgard-2500 (56 cycles). The superiority of the hybrid Li-SPOD GPE becomes more prominent when the current density increases to 2 mA/cm^2. That is, the hybrid GPE-based cell can maintain stable CEs of higher than 97% for 58 cycles, while the CEs of liquid electrolyte-based cell decline to ~95% at the 14th cycle, and dramatically decline at the 43rd cycle. At the highest current density of 3 mA/cm^2, the cell using the PP separator entirely loses

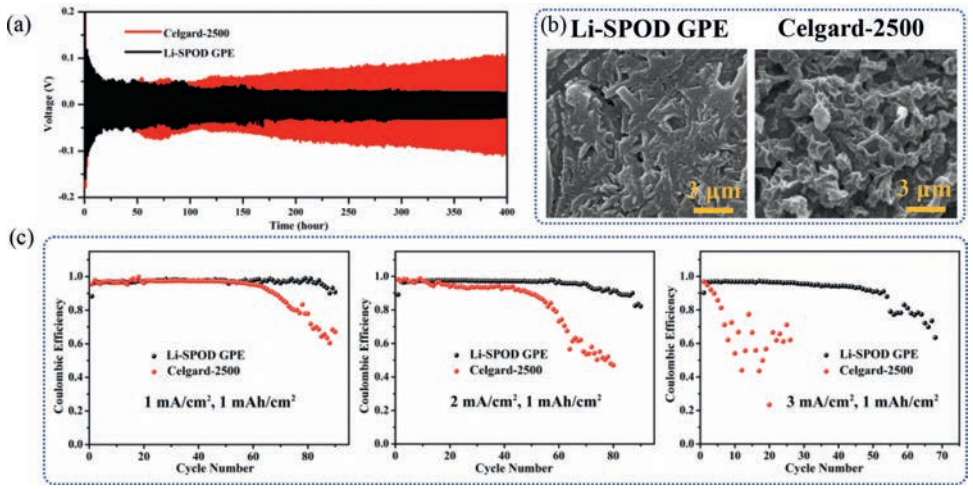

Fig. 4. (a) Voltage profiles of the Li-Li cells, (b) SEM images of Li electrodes of the Li-Li cells after 400 h cycling, and (c) Coulombic efficiencies of the Cu-Li cells at various rates in the long-term cycling processes.

its cycling stability from the very beginning. In sharp contrast, the cell with the hybrid Li-SPOD GPE is still able to cycle for 42 cycles with relatively steady CEs of higher than 94%. The initial low CEs of ~90% for the hybrid GPE-based Cu-Li cells at all the current densities are ascribed to irreversible electrochemical doping of the oxadiazole groups studied in our previous work [28]. The doping behavior is also observed in the initial stabilization processes of the Cu electrodes (Fig. S11 in Supporting information), where the depositing capacity onto the Cu electrode with the Li-SPOD GPE (0.0779 mAh) is more than 4 times higher than that with Celgard-2500 (0.0151 mAh) in the first cycle due to the electrochemical doping of the oxadiazole groups.

In summary, a nanofibrous hybrid GPE based on a novel polymeric sulfonate, Li-SPOD, and LiTFSI ether liquid electrolyte was successfully prepared. The Li-SPOD simultaneously with a high sulfonation degree and high molecular weight is synthesized through a simple one-pot method, and can be easily processed into a mechanically robust free-standing membrane with outstanding heat resistance. The electron-withdrawing oxadiazole ring and oxadiazole ring-Li^+ complex, and alkalescent N, O heteroatoms in Li-SPOD macromolecular chains are beneficial to the ionic dissociation of the -SO_3Li groups and cationic transference. The hybrid Li-SPOD GPE exhibits superior interfacial compatibility with lithium anodes, wider ESW, much higher σ and t_{Li^+} compared with the pure LiTFSI liquid electrolyte filled in the PP separator. The hybrid Li-SPOD GPE effectively alleviates lithium dendrites, and hence remarkable performance improvements are achieved in the cycling of $LiFePO_4$-Li, Li-Li and Cu-Li cells, implying a great application potential in rechargeable LMBs.

Declaration of competing interest

The authors declare that they have no known competing financial interests or personal relationships that could have appeared to influence the work reported in this paper.

Acknowledgements

This work was supported by the Fundamental Research Funds for Central Universities of China and the Key Research and Development Projects of Sichuan (No. 2020YFG0127). The authors gratefully acknowledge the State Key Laboratory of Polymer Materials Engineering, College of Polymer Science and Engineering, Sichuan University and the Analytical &Testing Centre of Sichuan University.

Supplementary materials

Supplementary material associated with this article can be found, in the online version, at doi:10.1016/j.cclet.2021.07.021.

References

[1] Q. Wang, H. Wang, J. Wu, et al., Nano Energy 80 (2021) 105516.
[2] C. Sun, J. Dong, X. Lu, et al., Adv. Energy Mater. 4 (2021) 2100594.
[3] A. Varzi, K. Thanner, R. Scipioni, et al., J. Power Sources 480 (2020) 228803.
[4] Z. Xie, Z. Wu, X. An, et al., Energy Storage Mater. 32 (2020) 386–401.
[5] M. Zhang, R. Liu, Z. Wang, et al., Chin. Chem. Lett. 31 (2020) 1217–1220.
[6] H. Dai, X. Gu, J. Dong, et al., Nat. Commun. 11 (2020) 643.
[7] W. Zhang, Z. Tu, J. Qian, et al., Small 14 (2018) 1703001.
[8] K. Jeong, S. Park, S.Y. Lee, J. Mater. Chem. A 7 (2019) 1917–1935.
[9] K. Deng, Q. Zeng, D. Wang, et al., J. Mater. Chem. A 8 (2020) 1557–1577.
[10] H. Zhang, C. Li, M. Piszcz, et al., Chem. Soc. Rev. 46 (2017) 797–815.
[11] H. Oh, K. Xu, H.D. Yoo, et al., Chem. Mater. 28 (2015) 188–196.
[12] J.J. Xu, Q.C. Liu, Y. Yu, et al., Adv. Mater. 29 (2017) 1606552.
[13] G. Chen, C. Niu, Y. Chen, et al., Solid State Ionics 341 (2019) 115048.
[14] Y. Wang, L. Fu, L. Shi, et al., ACS Appl. Mater. Interfaces 11 (2019) 5168–5175.
[15] B. Zhao, X. Lu, Q. Wang, et al., Chin. Chem. Lett. 31 (2020) 831–835.
[16] H. Li, X. Shen, H. Hua, et al., Solid State Ionics 347 (2020) 115246.
[17] X. Shen, H. Hua, H. Li, et al., Polymer (Guildf) 201 (2020) 122568.
[18] H. Hareendrakrishnakumar, R. Chulliyote, M.G. Joseph, S. Suriyakumar, A.M. Stephan, Electrochim. Acta 321 (2019) 134697.
[19] N. Shubha, H. Zhu, M. Forsyth, M. Srinivasan, Polymer (Guildf) 99 (2016) 748–755.
[20] K.M. Diederichsen, E.J. McShane, B.D. McCloskey, ACS Energy Lett. 2 (2017) 2563–2575.
[21] M.D. Tikekar, L.A. Archer, D.L. Koch, J. Electrochem. Soc. 161 (2014) A847–A855.
[22] H. Zhang, Y. Zhang, Z. Yao, et al., Electrochimi. Acta 204 (2016) 176–182.
[23] Y. Zhu, S. Xiao, Y. Shi, et al., Adv. Energy Mater. 4 (2014) 1300647.
[24] J.J. Yuan, C.C. Sun, L.F. Fang, et al., J. Energy Chem. 55 (2021) 313–322.
[25] C. Deng, Z. Wang, S. Wang, J. Yu, J. Mater. Chem. A 7 (2019) 12381–12413.
[26] V.S. Yashchenko, A.A. Pap, Y.V. Matveenko, V.K. Ol'khovik, Polym. Sci. Ser. B 58 (2016) 529–540.
[27] A. Abdolmaleki, M. Zhiani, M. Maleki, S. Borandeh, K. Firouz, Polymer (Guildf) 75 (2015) 17–24.
[28] Y. Yu, J. Zhu, H. Gao, et al., J. Appl. Polym. Sci. 137 (2020) 49406.
[29] J.L. Hedrick, Polym. Bull. 25 (1991) 543–550.
[30] J.L. Hedrick, R. Twieg, Macromolecules 25 (1992) 2021–2025.
[31] F.A. Bottino, G. Di Pasquale, P. Iannelli, Macromolecules 34 (2001) 34–37.
[32] D. Gomes, J. Roeder, M.L. Ponce, S.P. Nunes, J. Membr. Sci. 295 (2007) 121–129.
[33] S.O. Ilyin, A.Y. Yadykova, V.V. Makarova, V.S. Yashchenko, Y.V. Matveenko, Polym. Int. 69 (2020) 1243–1255.
[34] D. Gomes, J.C. Pinto, C. Borges, Polymer (Guildf) 44 (2003) 6223–6233.
[35] M. Guo, M. Zhang, D. He, et al., Electrochimi. Acta 255 (2017) 396–404.
[36] D. Xie, M. Zhang, Y. Wu, et al., Adv. Funct. Mater. 30 (2020) 1906770.
[37] G. Chen, F. Zhang, Z. Zhou, et al., Adv. Energy Mater. 8 (2018) 1801219.
[38] H. Lee, M. Yanilmaz, O. Toprakci, et al., Energy Environ. Sci. 7 (2014) 3857–3886.
[39] B. Cmca, C. Yhl, C. Jhk, et al., Energy Storage Mater. 22 (2019) 346–375.
[40] Y. Ding, X. Shen, J. Zeng, et al., Solid State Ionics 323 (2018) 16–24.
[41] Y.T. Weng, H.W. Liu, A. Pei, et al., Nat. Commun. 10 (2019) 5824.
[42] D. Li, H. Wang, L. Luo, et al., ACS Appl. Energy Mater. 4 (2021) 879–887.

[43] H. Yin, C. Han, Q. Liu, et al., Small (2021) 2006627.
[44] X. Chen, Y.K. Bai, C.Z. Zhao, et al., Angew. Chem. Int. Ed. 132 (2020) 11288–11291.
[45] R. Rohan, Y. Sun, W. Cai, et al., J. Mater. Chem. A 2 (2014) 2960–2967.
[46] C. Li, B. Qin, Y. Zhang, et al., Adv. Energy Mater. 9 (2019) 1803422.
[47] Z. Wang, W. Huang, J. Hua, et al., Small Methods 4 (2020) 2000082.
[48] Y. Huang, Y. Huang, B. Liu, et al., Electrochimi. Acta 286 (2018) 242–251.
[49] H. Zhang, Y. Zhang, T. Xu, et al., J. Power Sources 329 (2016) 8–16.
[50] Q. Yun, Y.B. He, W. Lv, et al., Adv. Mater. 28 (2016) 6932–6939.
[51] S.S. Zhang, J. Power Sources 231 (2013) 153–162.
[52] C. Brissot, M. Rosso, J.N. Chazalviel, S. Lascaud, J. Power Sources 81-82 (1999) 925–929.
[53] A. Hussain, D. Li, Y. Luo, et al., J. Membr. Sci. 605 (2020) 118108.
[54] F. Shen, K. Wang, Y. Yin, et al., J. Mater. Chem. A 8 (2020) 6183–6189.
[55] J. Lang, Y. Long, J. Qu, et al., Energy Storage Mater. 16 (2019) 85–90.
[56] H. Zhang, C. Shen, Y. Huang, et al., Appl. Surf. Sci. 537 (2021) 147983.
[57] S. Xiong, K. Xie, Y. Diao, et al., Electrochim. Acta 83 (2012) 78–86.